Enhanced contrast and depth resolution in polarization imaging using elliptically polarized light

Susmita Sridhar, Anabela da Silva

Enhanced contrast and depth resolution in polarization imaging using elliptically polarized light

Susmita Sridhar
Anabela Da Silva

Enhanced contrast and depth resolution in polarization imaging using elliptically polarized light

Susmita Sridhar[a,b,*] **and Anabela Da Silva**[a]
[a]Aix–Marseille Université, CNRS, Centrale Marseille, Institut Fresnel, UMR 7249, 13013 Marseille, France
[b]Institut de Ciències Fotòniques, Universitat Politècnica de Catalunya, 08860 Castelldefels, Barcelona, Spain

Abstract. Polarization gating is a popular and widely used technique in biomedical optics to sense superficial tissues (colinear detection), deeper volumes (crosslinear detection), and also selectively probe subsuperficial volumes (using elliptically polarized light). As opposed to the conventional linearly polarized illumination, we propose a new protocol of polarization gating that combines coelliptical and counter-elliptical measurements to selectively enhance the contrast of the images. This new method of eliminating multiple-scattered components from the images shows that it is possible to retrieve a greater signal and a better contrast for subsurface structures. *In vivo* experiments were performed on skin abnormalities of volunteers to confirm the results of the subtraction method and access subsurface information. © *The Authors. Published by SPIE under a Creative Commons Attribution 3.0 Unported License. Distribution or reproduction of this work in whole or in part requires full attribution of the original publication, including its DOI.* [DOI: 10.1117/1.JBO.21.7.071107]

Keywords: elliptically polarized light; light propagation in tissues; turbid media; medical and biological imaging.

Paper 150648SSR received Oct. 4, 2015; accepted for publication Jan. 8, 2016; published online Feb. 11, 2016.

1 Introduction

Driven by its biomedical potential, polarimetry and the use of its approaches for biological tissue assessment have received considerable attention. The interest in this type of imaging has grown due to the fact that, unlike conventional techniques based mainly on the exploitation of attenuating contrasts, polarimetric methods are very sensitive to the structure of the environment, operate by excluding light that is multiply-scattered and use the light that has kept its initial polarization.[1] The effect of scattering on the polarization state of light has been found very useful for the imaging of surface or subsurface structures in scattering media, and for transmission imaging of deep structures.[2] It has also been shown that the optical properties of turbid tissue, including the reduced scattering coefficient, can be determined from diffusely scattered polarized light.[3] The incorporation of polarimetric imaging in more conventional techniques such as microscopy or optical coherence tomography helps in the extraction of precise information such as on collagenous tissue structure (eye,[4] skin,[5] and cervix[6]). Promising studies of polarimetric examination of tissues were carried out in dermatology,[7–13] where melanomas or other lesions (lupus) were characterized by various polarimetric indicators (depolarization and birefringence). However, in a complex random medium-like tissue, numerous complexities due to multiple scattering and simultaneous occurrences of many scattering and polarization events present formidable challenges both in terms of accurate measurements and in terms of analysis of the tissue polarimetry signal.

These techniques are based on the fact that the polarization is lost depending on the tissue's scattering properties. The backscattered light thus contains a mixture of polarized photons that have undergone a limited number of scattering events and depolarized light. Polarized light can be extracted by a simple image subtraction method[14] (a) for moving beyond the specular and probing more deeply (e.g., using crossed linear polarizers); or (b) for selecting the specular photons (e.g., using colinear polarizers). For tissue examination, a widely used technique is the detection via the crosslinear imaging channel to get rid of the mirror reflections.[15] Linear polarization gating[1,7,16] is limited to the surface examination of tissues. The underlying principle for linear polarization gating as a depth selective technique can be summarized as: the photons which are scattered (or re-emitted) from deeper tissue layers undergo multiple scattering events and are depolarized to a larger extent. For examining tissues deeper, the use of circular polarization was introduced by Morgan and Stockford[17] and they demonstrated that subtraction of images taken in cocircular illumination/detection configuration and crosslinear illumination/detection allowed for the extraction of circular polarization maintaining light and the elimination of specular-reflected photons. Due to the effect of "polarization memory,"[18,19] the depth probed by circular polarization is larger than that with linear polarization because the polarization of circularly polarized light is indeed maintained through a larger number of scattering events than that of linearly polarized light in Mie scatterers such as biological tissues. This effect was further investigated and verified by Monte Carlo simulations in a semi-infinite medium.[20] The simulation results concluded that the mean visitation depth for linearly polarized light [~2 mean free paths (MFPs)] is smaller than that of circularly polarized light (~10 MFPs). They also found that elliptical polarization can be tuned between linear and circular polarization to reach different penetration depths. It has been demonstrated that the average depth into which elliptically polarized light can penetrate is between that of linearly and circularly polarized light.[21,22] This technique allows screening the tissue at specific depths ranging between the surface and a maximum depth defined by the maximum penetration depth of the circularly polarized photons.

*Address all correspondence to: Susmita Sridhar, E-mail: susmita.sridhar@fresnel.fr

In this paper, we have chosen to develop this approach because it allows for noncontact tissue examination over a large (wide-field) region of interest (ROI) with low-cost instrumentation. In addition and in comparison to practiced techniques, we introduce a subtraction method involving the co- and counter-elliptically polarized light to probe subsurface volumes. The principle is demonstrated with phantom experiments on Intralipid® and *ex vivo* tissue. The extent of this method is also substantiated with *in vivo* experiments on human skin.

2 Polarization Gating with Elliptically Polarized Light

Elliptical polarization has seldom been used in polarization gating but has been catching up especially in the field of optical biopsy.[23] This form of polarization gating has two reasonable advantages over linear polarization gating (see Fig. 1): (a) it undergoes a change in helicity by reflection, which eliminates the specular reflection through co-elliptical detection; (b) also, elliptically polarized light retains its polarization state for a larger number of scattering events than that of linearly polarized light.

Figure 1 shows the types of photons acquired when polarized light is illuminated linearly or elliptically. Based on previous works,[17,19,22,24] we adapted the polarization scheme of illumination/detection with four different imaging channels as shown in Table 1.

Note that some recent studies have demonstrated that circularly polarized light is more depolarized in Intralipid®[25] and tissue samples[26] than linearly polarized light. The depolarization factor, that is the ratio between the intensity of detected polarized light to intensity of illuminated polarized light, has not been considered for our studies and only the signal containing polarization maintaining volume is taken into consideration. The raw signal collected through a given polarization gate, after subtraction of a proper amount of depolarized light, is related to a well-defined probing depth, no matter the amount of polarized signal left.
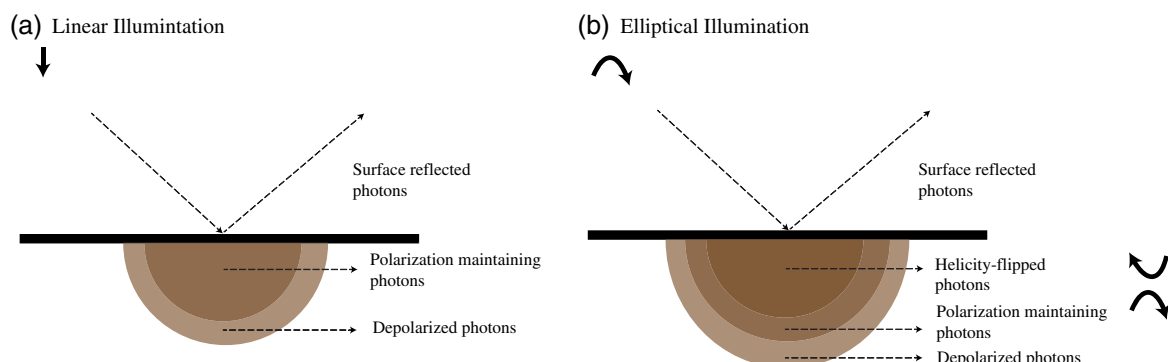
Polarization gating methods concentrate on subtracting the background from the images to improve the polarized signal. In practice, a simple subtraction between colinear and crosslinear imaging channels, $C1 - C2$, allows the separation of the surface contribution from the multiple-scattered part (coming from deeper volumes), MS_L, resulting in an enhancement of the surface image ($S_L + P_L$). However, linear polarization gating alone does not allow simultaneous filtering of mirror reflections and multiple-scattered light. To overcome this problem, the use of circularly polarized light was adopted,[17,19] wherein the

Table 1 Back-scattered photon characteristics measured in different imaging channels.

Channel	Illumination	Detection	Light characteristics
$C1$	Linear	Linear	Surface-reflected (S_L) + polarization maintaining (P_L) + multiple-scattered photons (MS_L)
$C2$	Linear	Cross-linear	Multiple-scattered photons (MS_L)
$C3$	Elliptical	Co-elliptical	Polarization-maintaining (P_E) + multiple-scattered photons (MS_E)
$C4$	Elliptical	Counter-elliptical	Surface-reflected (S_E) + multiple-scattered photons (MS_E)

crosslinear fraction was subtracted from the co-elliptical images, $C3 - C2$, to access subsurface volumes (with the assumption that the subtraction nullifies the multiple-scattered photons from both channels and gives only elliptical polarization maintaining photons, P_E[27]). This method, referred to as subtraction method 1 in this paper, however, removes an amount of linearly multiple-scattered photons much greater than elliptically multiple-scattered photons. This over-subtraction leads to the loss of some valuable information at the subsuperficial layers.

To overcome this problem and to account for the fact that the multiple-scattered photons arising from linear polarization gating and circular polarization gating are different from each other in fraction, we have devised a new method (referred to as subtraction method 2 in this paper) to equate and eliminate the background by subtraction. To obtain the polarization maintaining photons from the elliptical channels, a subtraction between the elliptical channels is performed ($C3 - C4$) to eliminate the elliptically multiple-scattered photons. After this subtraction, a mixture of backscattered elliptical polarization maintaining photons and the elliptical surface-reflected photons is obtained. To preserve only the polarization maintaining photons, we can combine the residuals of linear polarization gating, $C1 - C2$, and that of elliptical channels, $C3 - C4$. This gives us a mixture of the surface reflected and polarization maintaining photons from linear and elliptical polarizations ($P_E - S_E + P_L + S_L$). At non-normal incidence, the quantities of surface-reflected photons from linear and elliptical polarization are different from each other, with a larger contribution from the former (which can be measured theoretically and experimentally). This can

(a) Linear Illumination

Surface reflected photons

Polarization maintaining photons

Depolarized photons

(b) Elliptical Illumination

Surface reflected photons

Helicity-flipped photons

Polarization maintaining photons

Depolarized photons

Fig. 1 Schematic representation of (a) linear illumination and (b) elliptical illumination.

be verified by the fact that as we go from colinear channel to counter-elliptical channels, we are not only increasing the angle of elliptical polarization, but also changing the amount of reflected light projected in the plane of incidence (parallel or *P*-polarized) to that perpendicular to the plane of incidence (perpendicular or *S*-polarized). This change in the specular portion of the elliptical channels can be normalized to that of the linear channel by a factor, α, such that $S_E = \alpha S_L$. This α value is calculated as the ratio of surface-reflected components of counter-elliptical to colinear images, and it is computed experimentally on an ROI containing mostly the identified specular-reflection spot. Therefore, to eliminate these specular portions from the images, we can reduce the equation as

$$(C3 - C4) + \alpha(C1 - C2) = P_E + \alpha P_L. \tag{1}$$

This method allows us to obtain only the polarization maintaining photons with the elimination of background in terms of specular and multiple-scattered photons. In this paper, the two mentioned subtraction methods 1 and 2 are compared and illustrated with experiments on different types of samples.

3 Materials and Methods

3.1 Instrumentation

The experimental setup [Fig. 2(a)] is composed of a 250 W halogen light lamp (KL 2500 LCD, Schott AG, Germany) for illumination. The incident light is first wavelength-filtered with bandpass filters (532, 570, or 633 nm with bandwidth 10 ± 2 nm, Thorlabs®, Germany) and is then passed through a polarization state generator (PSG) composed of a linear polarizer (1 in., dichroic, extinction ratio 10,000:1, LPVISB100, Thorlabs®, Germany) and a quarter-wave plate (1 in., achromatic

zero-order wave plate for wavelength range 500 to 700 nm with a $\pi/2$ dephasing at 633 nm, SPD—Samoylov A.V., Ukraine), to produce elliptically polarized light. For detection, the reflected beam passes through a polarization state analyzer (PSA) composed of a quarter-wave plate (2 in., achromatic zero-order wave plate for wavelength range 500 to 700 nm with a $\pi/2$ dephasing at 633 nm, SPD—Samoylov A.V., Ukraine) and an analyzer (1 in., dichroic, extinction ratio 10,000:1, LPVISB100, Thorlabs®, Germany), to return to the state of polarization. The relative rotation angle between polarizers and quarter-wave plates is tuned such as to obtain the desired polarization modes for illumination and detection [Fig. 2(b) and Table 1]. The reflected beam then passes through a magnification lens (AC508-400 A-ML, Thorlabs®, Germany) and is detected by a CMOS camera (Orca Flash 4.0, Hamamatsu Photonics, Japan) with an objective (7000E, Laser Components SAS, France).

3.2 Calibration

The axes of the polarizer and analyzer were identified under transmission geometry by conventional extinction measurements (with the help of a reference polarizer whose transmission axis was known). While the polarizer and analyzer were in crossed configuration, either of the quarter-wave plates were placed in between to find their fast- and slow-axes, respectively. Once the axes of all the components were determined, the axes of the components were adjusted under reflectance geometry and experiments were conducted with Intralipid® samples for the generation of different ellipses. We use the polarizer/quarter-wave plate couple in the illumination path to generate different elliptically polarized illumination, by adjusting the angle, φ, between the fast-axis of the quarter-wave plate and the linear polarizers' axis. We then use another polarizer/quarter-wave
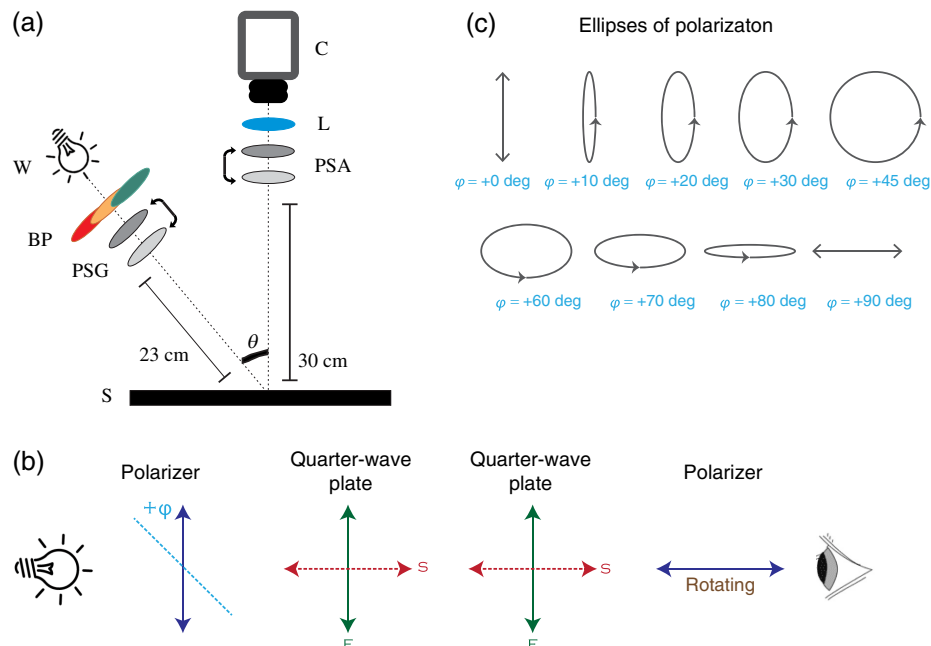
Fig. 2 (a) Schematic of the experimental setup where, W, white light source; BP, bandpass filters; PSG, polarization state generator composed of a polarizer and quarter-wave plate; θ, angle of incidence; PSA, polarization state analyzer composed of a quarter-wave plate and analyzer; L, magnification lens; C, CMOS camera with objective. (b) Schematic of generating ellipses when tuning the polarizers with the quarter-wave plates kept constant. (c) Ellipses of polarization produced when tuning the polarizers with the quarter-wave plates kept constant, where φ is the angle of elliptical polarization.

plate couple for detection and the ellipticity "φ" in the detection path is set to correspond to the same as in the illumination path. So for each measurement, we need to tune the two polarizer/quarter-wave plate couples to obtain the desired state of polarization for illumination and detection. Two different modes of tuning the polarizer/quarter-wave plate couple can be employed: (a) tuning just the polarizers with the quarter-wave plates kept constant and (b) tuning the polarizers and quarter-wave plates. The shape and orientation of the ellipses totally depend on the position of the quarter-wave plate. In this paper, all the experiments described have been performed using the first method, where only the polarizers are tuned and the quarter-wave plates are kept unchanged and is shown in Figs. 2(a) and 2(b). It is evident that the intensity and behavior of signals are very different depending on the shape of the ellipse for the two modes of tuning the polarizer/quarter-wave plate couple.

3.3 Samples and Medium

Different types of samples were used for calibration and validation of measurements illustrated in this paper. All the experiments were conducted in compliance with the directions of the local ethics committee. All procedures were in agreement with NIH guidelines.

i Liquid phantom: Intralipid®
The liquid phantom was composed of an aqueous Intralipid® (20%, Sigma-Aldrich, France) at adequate concentrations. The concentration of Intralipid® was adapted to match the optical properties of biological tissues, but with a scaling in size of the sample for macroscopic measurement of depth. The optical properties of Intralipid® 1% was determined by the integral reflectance method:[28] the absorption coefficient (μ_a) was considered negligible and a reduced scattering coefficient value of $\mu_{s'}(1\%) = 10.3 \pm 0.5$ cm^{-1} was estimated. According to the accuracy of our optical (magnification) and mechanical components, a 0.1% diluted solution was adopted, corresponding to $\mu_{s'}(0.1\%) = 0.95 \pm 0.05$ cm^{-1}, allowing depth measurements at a millimetric scale. The anisotropy factor of Intralipid® was estimated to a value of $g = 0.73$,[29] leading to a reduced scattering mean free path MFP$' = (1 - g)/\mu_{s'} \sim 2.8$ mm (that is $\sim$10 times longer than in biological tissues).

ii *ex vivo*: Neck of chicken
To check for biological tissue feasibility, a piece of chicken neck (bought from the supermarket, used as a biological phantom) pinned to a sample holder was used. The neck in particular was chosen due to the prominence of a blood vessel in the region. The superficial tissue was sufficiently hydrated with glycerin to track the mirror reflections.

iii *in vivo*: Human skin
The dorsal side of the hand (showing a mole/nevus) of a volunteer was illuminated under the given experimental conditions. A glass cover-slip was placed on the skin to track the specular reflections at the surface. The exposure dose was much below the maximum permissible exposure values in the visible wavelength range ($\sim$0.065 W/cm^{-2}) (Laser Institute of America 2000) and an informed consent was obtained from all subjects.

3.4 Image Processing

Images were acquired using HCImageLive Software (provided by Hamamatsu for CMOS camera ORCA Flash 4.0). The SNR was calculated as the ratio of the desired signal intensity to the background intensity [SNR $= 10 \log(I_s/I_n)$]. A sequence of 20 images were taken with an adapted exposure time per measurement in order to preserve a high SNR (35 dB) for each measurement. The noise was reduced by averaging these images. However, for need of comparison of different measurements, the data are expressed per unit exposure time. An image registration, which corrected translational and rigid body movements in the images, was carried out using *imregister* and *imreconfig* functions in MATLAB® R2015a. After correcting for movement, the images were averaged to a single mean-image. These mean-images were then subtracted based on one of the methods described in Sec. 2.
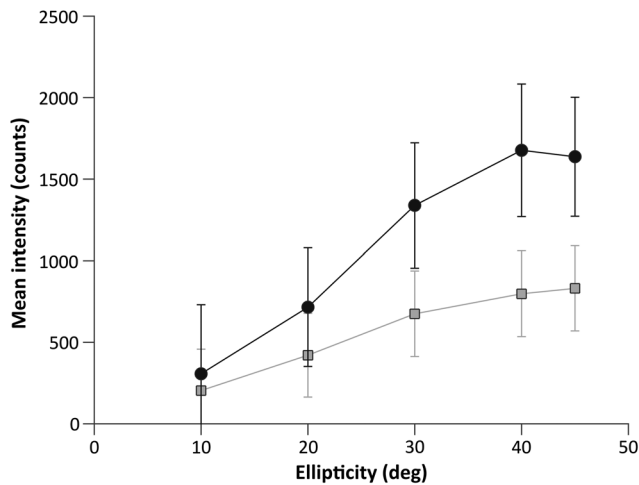
4 Results and Discussion

The different phantoms were examined under the imaging channels described, and the images were then processed and compared for the two subtraction methods in question. The relation between the image contrast and the state of polarization was examined and analyzed.
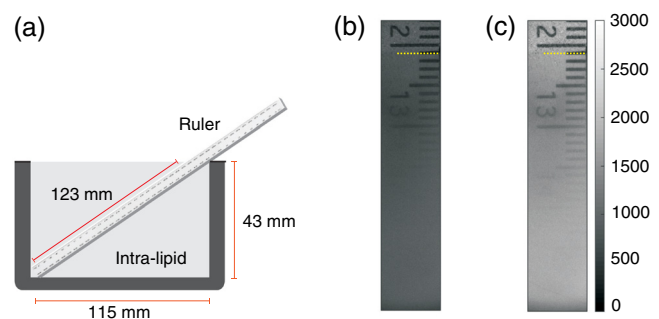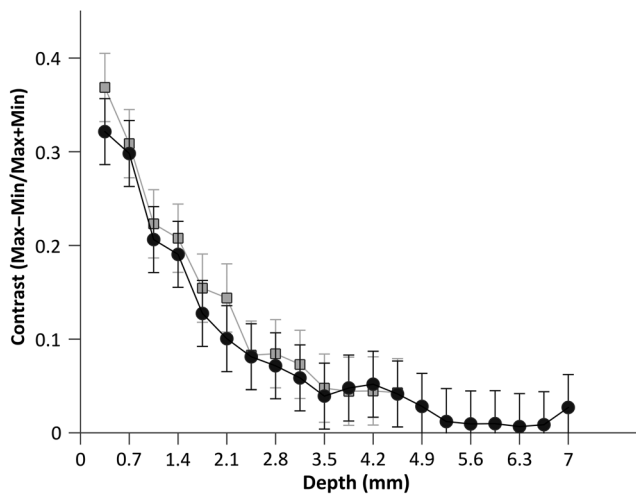

Fig 3 Results of the Intralipid® experiments: (a) ruler placed obliquely in a tank containing Intralipid® solution, (b) elliptical channel image at 45 deg after subtraction method 1, (c) elliptical channel image at 45 deg after subtraction method 2. (b) and (c) have a common colorbar represented at the right edge of the figure. Yellow-dotted line represents the Intralipid®–air interface. Each graduation on the ruler (i.e., 1 mm) corresponds to 0.35 mm in actual depth. Wavelength: 633 nm.
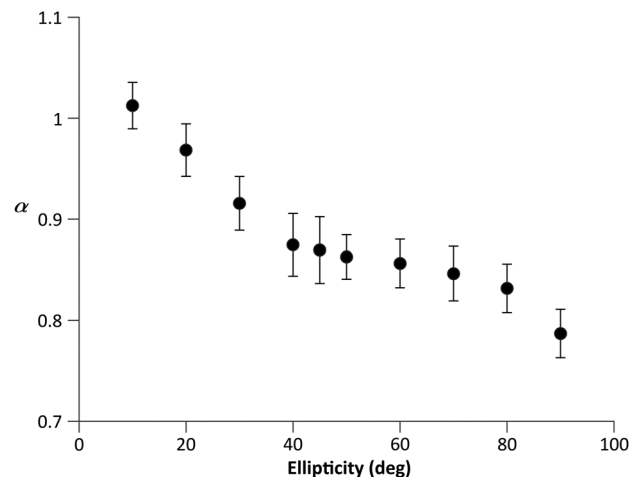

Fig. 4 Trend of α factor as a function of ellipticity for 0.1% Intralipid® experiments.

Fig. 5 Signal intensity of 0.1% Intralipid® when performing subtraction with (a) method 1 (squares) and (b) method 2 (circles). Standard deviation bars are also shown. Image exposure time: 1000 ms.

Fig. 6 Depth probed with elliptic channel at 45 deg for 0.1% Intralipid® when performing subtraction with (a) method 1 (squares) and (b) method 2 (circles). Standard deviation bars are also shown. Image exposure time: 1000 ms.
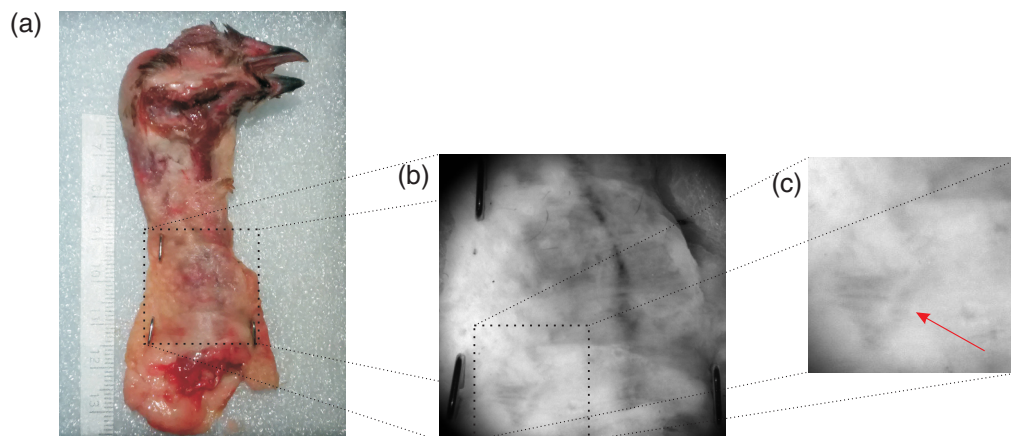
4.1 Intralipid®

Experiments on the Intralipid® were conducted to compare the two background subtraction methods and served as a sample for calibrating the setup. A plastic ruler had been placed obliquely in a tank containing the diluted Intralipid® as shown in Fig. 3(a) and imaged at different ellipticities to observe the signal coming from different depths.

The α factor for removing the specular component was calculated experimentally as follows: a series of 100 images were taken at channel $C1$ and channel $C4$ (which contain the respective linear and elliptical specularly reflected components). The ROI containing an identified specular spot was averaged to get a mean value in both $C1$ and $C4$. α was then calculated as the ratio of the mean specular values of elliptical to linear channels. This value was found to decrease with the increase in the angle of the elliptical channel. The value and range of α depend on the sample used. Figure 4 shows that, for Intralipid® 0.1% measurements, α was found in the range 1.01 to 0.78, for ellipticities 0 to 90 deg.

The mean intensity of images with subtraction methods 1 and 2 is shown in Fig. 5. It shows that with subtraction method 2, there was a higher signal intensity, especially for larger angles of elliptical polarization (a 110% increase in angles 30 and 40 deg) in the imaging channels. The signal intensity showed an increase from linear to 40 deg elliptical polarization, reaching a plateau after 40 deg (close to circular polarization).

Figure 6 shows the contrast as a function of depth probed (in mm) for the two subtraction methods. The contrast was measured using the ratio $(I_{max} - I_{min})/(I_{max} + I_{min})$, where I represents the mean value of intensity. In terms of depth, subtraction method 1 allowed us to have a reasonable contrast up to 13 graduations (i.e., 4.55 mm), as compared to subtraction method 2, which allowed a good contrast up to 20 graduations (i. e., 7 mm). This clearly shows that there is a substantial increase in percentage of signal intensity and in the reachable depth when background subtraction is achieved using subtraction method 2. This is also very evident visually when comparing Figs. 3(b) and 3(c), where 3(c) appears to have a better contrast than 3(b).

This experiment shows that polarized light can be collected up to 7 mm in depth (corresponding to 0.7 mm in biological tissues).

Fig. 7 *Ex vivo* sample of neck tissue of a chicken: (a) Top view of the sample. (b) Crosslinear image of a part of the neck under study. (c) Zoom-out (crosslinear) of a section containing a vessel indicated by the red arrow. Images taken in white light. Thickness of epidermis: ~0.5 to 0.8 mm (determined by dissection postimaging).

4.2 Ex Vivo Tissue

The *ex vivo* experiments were conducted on a piece of neck of a chicken (see Fig. 7) and illustrated the feasibility of this study in other kinds of tissues. In the ROI projected in Figs. 7(c) and 8, there is evidence of a vessel appearing diagonally in the cross-linear image. This vessel, which is not visible in the colinear image, (i.e., it lies in the subsurface) can only be seen in the contrasts of elliptic channels at 10, 20, 30, 40, 45, and 50 deg [in Figs. 8(d)–8(i)]. The presence of wrinkles (caused due to the attachment of the tissue with metallic pins) can also be seen pronounced in Figs. 8(e)–8(h). Validating our statements, elliptic channels up to 45 deg show the presence of deeper lying structures, whereas smaller angles, i.e., smaller elliptic channels, show superficial structures or structures close to the surface.

4.3 In Vivo Tissue

4.3.1 Human skin

A mole on the dorsal side of a volunteer's hand was observed (see Fig. 9). Figure 10 shows the contrast of subtraction method 2 performed on skin images. It can be observed that the mole is quite clearly outlined in the elliptic channels [Figs. 10(c)–10(l)], but it is negative and depicts the depolarized photons. On the other hand, it can be seen that the intensity of a polarizing structure (seen toward the right edge of each figure) increases from
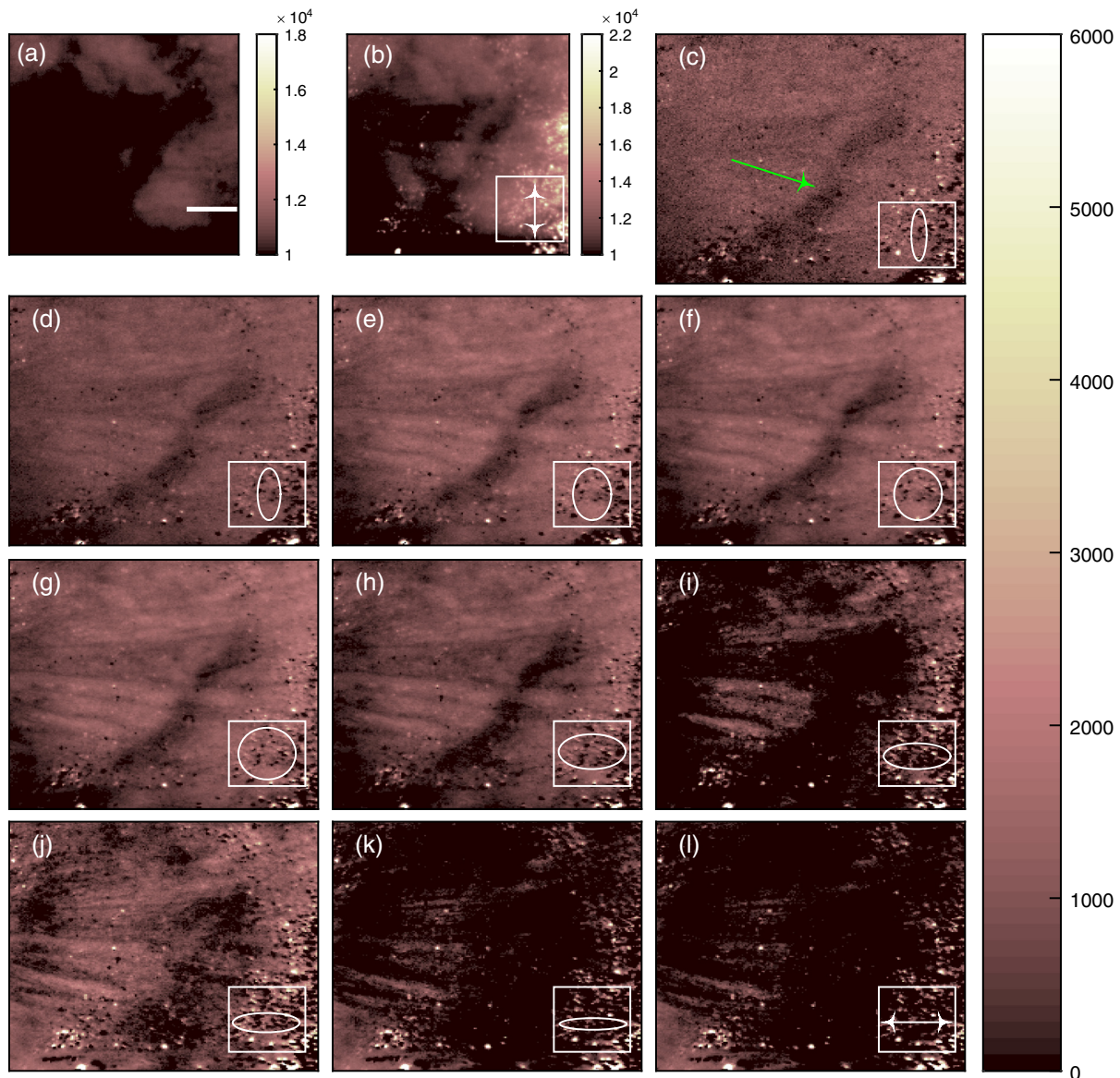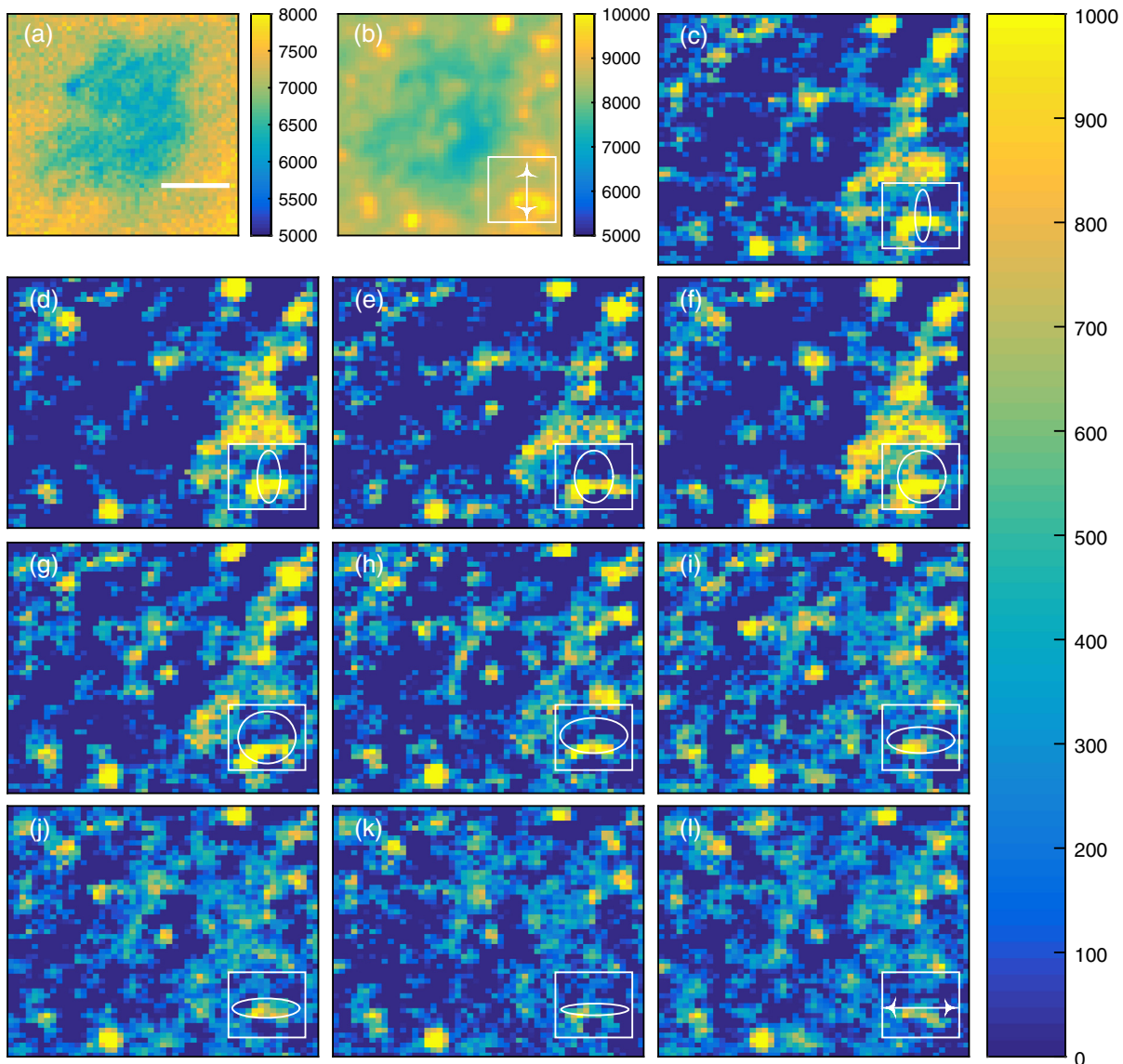

Fig. 8 Contrast for linear and elliptic channels for *ex vivo* measurements on neck tissue of a chicken. (a) The cross-linear image. (b) The contrast of the subtraction of linear (co and cross) channels. (c) to (l) The contrasts for the subtraction of elliptic (co and counter) channels 0, 10, 20, 30, 40, 45, 50, 60, 70, 80, and 90 deg, respectively. Scale bar: (a) 2 mm. Wavelength: 633 ± 10 nm. Image exposure time: 1000 ms. Behavior of the polarized light (linear/elliptical) is represented at the bottom-right corner of each figure. (a) and (b) are raw images and have their own colorbar. (c) to (l) have a common colorbar represented at the right border of the image. Green arrow in (c) indicates the presence of the vessel.
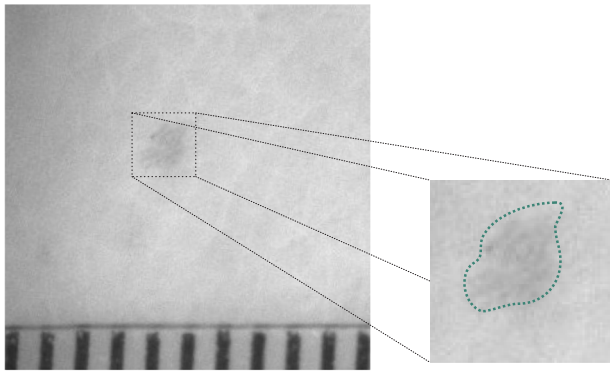
Fig. 9 Dorsal side of a hand along with a zoom-out of the mole which was studied for the *in vivo* experiments. A ruler with graduations in millimeters is seen at the bottom of the image. Images taken in white light.

Figs. 10(c) to 10(f). Inversely, the intensity of this structure is observed to be decreasing from Figs. 10(h) to 10(l). There is also the appearance of different structures within the space of the mole from Figs. 10(h) to 10(l), indicating that these structures are polarizing in a direction different from the colinear direction (vertical) and horizontal to the polarization at 90 deg (back to linearly polarized light, but in the opposite direction). This behavior conforms with that of the ellipses shown in Fig. 2(c). Due to the effects of image subtraction, the SNR of the resulting channel images is smaller than that of the measured images. Using basic image processing should allow to reduce the noise content of the images. The depolarization/negativity of deeper lying structures could be mainly due to very high specular components from the elliptical channels. This can be avoided by improvization of the setup with the addition of a telecentric

Fig. 10 Contrast for linear and elliptic channels for *in vivo* measurements on dorsal side of a human hand. (a) Histogram of the crosslinear channel tracing the shape of the mole. (b) Contrast of the subtraction of linear (co and cross) channels. (c) to (l) The contrasts for the subtraction of elliptic (co and counter) channels 0, 10, 20, 30, 40, 45, 50, 60, 70, 80, and 90 deg, respectively. Scale bar: (a) 0.5 mm. Wavelength: 633 ± 10 nm. Image exposure time: 1500 ms. Behavior of the polarized light (linear/elliptical) is represented at the bottom-right corner of each figure. (a) and (b) are raw images and have their own colorbar. (c) to (l) have a common colorbar represented at the right border of the image.

objective that converges the illumination beam and provides a more homogeneous illumination.

5 Conclusions

In this paper, we test the feasibility of depth examination by tuning the state of polarization in four imaging channels, and compare two systems of image subtraction with experiments on calibrated Intralipid® phantoms, *ex vivo*, and *in vivo* tissues. Intralipid® measurements confirm that subtraction method 2 involving all the four imaging channels is superior to subtraction method 1 because: (a) there is higher signal intensity, (b) there is a higher contrast in surface structures, and (c) it allows probing a depth of 7 mm. Our phantom experiments show that this method can be used to probe tissues in depth up to at least 0.7 mm, which offers the possibility of screening a variety of layered biological tissues such as the skin as tested here.

Ex vivo experiments on chicken neck and human skin experiments conform with the above conclusions, and show higher signal intensity and higher contrast of some structures with elliptic channels (from 0 to 45 deg) probing subsurface structures.

Further work includes removal of the specular reflection at the surface using better and more adapted optical clearing agents. This could lead to a more efficient isolation of the polarization maintaining photons. In addition, the crosslinear channel has the highest SNR, and this needs to be improved for the elliptic channels to get a better contrast of the subsurface structures.

Depending on optical properties of the medium, the exact depth and extent of these subsurface volumes can be calculated. With advancements in the setup and better signal processing, this method should allow for imaging deeper volumes at specific/user-defined depths. This method could be very valuable in the field of noninvasive blood flow-sensing, detection of low-lying tumors, or other skin abnormalities.

References

1. J. M. Schmitt, A. H. Gandjbakhche, and R. F. Bonner, "Use of polarized-light to discriminate short-path photons in a multiply scattering medium," *Appl. Opt.* **31**(30), 6535–6546 (1992).
2. M. P. Rowe et al., "Polarization-difference imaging—a biologically inspired technique for observation through scattering media," *Opt. Lett.* **20**(6), 608–610 (1995).
3. A. H. Hielscher, J. R. Mourant, and I. J. Bigio, "Influence of particle size and concentration on the diffuse backscattering of polarized light from tissue phantoms and biological cell suspensions," *Appl. Opt.* **36**, 125–135 (1997).
4. M. G. Ducros et al., "Primate retina imaging with polarization-sensitive optical coherence tomography," *J. Opt. Soc. Am. A* **18**(12), 2945–2956 (2001).
5. T. Yasui, Y. Tohno, and T. Araki, "Characterization of collagen orientation in human dermis by two-dimensional second-harmonic-generation polarimetry," *J. Biomed. Opt.* **9**(2), 259–264 (2004).
6. S. Bancelin et al., "Determination of collagen fiber orientation in histological slides using Mueller microscopy and validation by second harmonic generation imaging," *Opt. Express* **22**(19), 22561–22574 (2014).
7. S. G. Demos and R. R. Alfano, "Optical polarization imaging," *Appl. Opt.* **36**, 150–155 (1997).
8. S. L. Jacques, J. C. Ramella-Roman, and K. Lee, "Imaging skin pathology with polarized light," *J. Biomed. Opt.* **7**(3), 329–340 (2002).
9. I. M. Stockford et al., "Analysis of the spatial distribution of polarized light backscattered from layered scattering media," *J. Biomed. Opt.* **7**(3), 313–320 (2002).
10. I. M. Stockford and S. P. Morgan, "Application of a look-up table to polarized light imaging for characterising skin," presented at *Saratov Fall Meeting 2004: Optical Technologies in Biophysics and Medicine VI*, Vol. 5771, pp. 151–158 (2005).
11. S. P. Morgan et al., "Modelling and instrumentation for polarized light imaging and spectroscopy of scattering media—art. no. 604712," in *Fourth Int. Conf. on Photonics and Imaging in Biology and Medicine, Pts 1 and 2*, Vol. 6047, pp. 4712 (2006).
12. D. Kapsokalyvas et al., "Spectral morphological analysis of skin lesions with a polarization multispectral dermoscope," *Opt. Express* **21**(4), 4826–4440 (2013).
13. A. Pierangelo et al., "Polarimetric imaging of uterine cervix: a case study," *Opt. Express* **21**(12), 14120 (2013).
14. S. L. Jacques, J. R. Roman, and K. Lee, "Imaging superficial tissues with polarized light," *Lasers Surg. Med.* **26**(2), 119–129 (2000).
15. R. R. Anderson, "Polarized-light examination and photography of the skin," *Arch. Dermatol.* **127**(7), 1000–1005 (1991).
16. S. G. Demos, H. B. Radousky, and R. R. Alfano, "Deep subsurface imaging in tissues using spectral and polarization filtering," *Opt. Express* **7**(1), 23–28 (2000).
17. S. P. Morgan and I. M. Stockford, "Surface-reflection elimination in polarization imaging of superficial tissue," *Opt. Lett.* **28**(2), 114–116 (2003).
18. F. C. MacKintosh et al., "Polarization memory of multiply scattered light," *Phys. Rev. B* **40**, 9342–9345 (1989).
19. S. P. Morgan and M. Ridgway, "Polarization properties of light backscattered from a two layer scattering medium," *Opt. Express* **7**(12), 395–402 (2000).
20. S. Rehn et al., "Depth probing of diffuse tissues controlled with elliptically polarized light," *J. Biomed. Opt.* **18**, 016007 (2013).
21. A. Da Silva et al., "Depth selectivity in biological tissues by polarization analysis of backscattered light," *Proc. SPIE* **8172**, 817205 (2011).
22. A. Da Silva, C. Deumié, and I. Vanzetta, "Elliptically polarized light for depth resolved optical imaging," *Biomed. Opt. Express* **3**(11), 2907 (2012).
23. B. Kunnen et al., "Application of circularly polarized light for non-invasive diagnosis of cancerous tissues and turbid tissue-like scattering media," *J. Biophotonics* **8**(4), 317–323 (2015).
24. X. Feng, L. Sun, and E. Zhang, "Depth selectivity for the assessment of microstructure by polarization studies," *Biomed. Opt. Express* **4**(6), 958–966 (2013).
25. M. K. Swami et al., "Effect of gold nanoparticles on depolarization characteristics of intralipid tissue phantom," *Opt. Lett.* **38**(15), 2855–2857 (2013).
26. M. K. Swami et al., "Size-dependent patterns in depolarization maps from turbid medium and tissue," *Appl. Opt.* **53**(27), 6133 (2014).
27. S. L. Jacques, "Corrigendum: optical properties of biological tissues: a review," *Phys. Med. Biol.* **58**, 5007–5008 (2013).
28. L. Gobin, L. Blanchot, and H. Saint-Jalmes, "Integrating the digitized backscattered image to measure absorption and reduced-scattering coefficients in vivo," *Appl. Opt.* **38**(19), 4217–4227 (1999).
29. H. J. Van Staveren et al., "Light scattering in intralipid-10% in the wavelength range of 400–1100 nm," *Appl. Opt.* **30**(31), 4507–4514 (1991).

Susmita Sridhar is currently pursuing her doctoral studies as part of the Europhotonics Erasmus Mundus Joint PhD Program at Institut Fresnel, Marseille and ICFO, Barcelona (Expected graduation September 2016). Her research interests are focused in biomedical optics, more specifically on polarization gating imaging for depth resolution in biological tissues. She has a joint MSc degree in biomedical engineering from Lübeck University of Applied Sciences and University of Lübeck, Germany.

Anabela Da Silvas main research field is biomedical optics, with a special focus on diffuse optical tomography, polarization gating imaging, and photoacoustic imaging. She holds a PhD in optics and photonics (Pierre and Marie Curie University, Paris, France). After a post-doc at Harvard Medical School/Massachusetts General Hospital, she worked as a researcher at CEA-LETI (Grenoble, France). Since 2008 she is a senior researcher at French National Research Center.